Salty Matters

John Warren -Sunday July 31h, 2016

Silica mobility and replaced evaporites: 2 - Silicified anhydrite nodules

Introduction

Postdepositional silicification of sulphate evaporites, that is the precipitation of authigenic silica as a replacement of a $CaSO_4$ host, is the focus of this article, but can be considered a subtopic of the broader styles of silica deposition and silicification that have occurred throughout the geological record from the Precambrian to the Quaternary (Knauth and Epstein 1976; Bustillo 2010). The next article will extend the silica -precipitate discussion back in time across the Proterozoic and into the Archean and consider the influences of atmospheric evolution and seawater chemistry on the styles of silica rocks across deep time. At this point in our discussion, a few relevant geological and mineralogical definitions are needed (see Bustillo, 2010 and Marin-Carbonne et al for more detail). Silica rock is a general term used to define any rock composed mainly of SiO_2. In the strict sense, "chert" is used to define a silica rock made primarily of quartz, plus small amounts of opaline minerals, whereas the term "opal" is used to indicate both a mineral and rock. Cherts are sedimentary rocks formed either by direct precipitation from hydrothermal fluids or seawater (known as C-cherts) or by silicification of precursor material (S-cherts). That is, C-cherts are the result of orthochemical precipitation from seawater (or any Si-rich fluid) and S-cherts are the result of the replacement of a precursor lithology (van den Boorn et al. 2010). This precursor can be evaporitic or volcanogenic sediment (Marin-Carbonne et al., 2014) This article emphasises S-chert examples from the Phanerozoic saline settings, where silica is a secondary phase replacing a pre-exisiting evaporite nodule or crystal. This style of authigenic silica is a common diagenetic constituent in evaporitic carbonates, and occurs in a variety of crystal forms and morphologies (Folk and Pittman 1971; Chowns and Elkins 1974; Knauth 1979; Milliken 1979; Geeslin and Chafetz 1982; Chafetz and Zhang 1998; Scholle and Ulmer-Scholle 2003).

Authigenic silica (S-cherts) can form by: (1) Diagenetic recrystallization of an amorphous silica precursor (Hesse 1989; Knauth 1994); (2) Direct precipitation from aqueous solutions (Mackenzie and Gees 1971; Guidry and Chafetz 2002; Marin et al. 2010); and (3) Direct replacement of pre-existing olcanogenic, carbonate or evaporite host (Hesse 1989; Knauth 1994). Several possible chemical explanations have been suggested to drive the replacement. These include silica precipitation induced by a local decrease in pH that is caused by either biological production of CO_2 (Siever 1962), oxidation of sulfide into sulphate (Clayton 1986; Chafetz and Zhang 1998), and mixing of marine and meteoric waters (Knauth 1979).

Types and traits of authigenic silica and chert

The previous article in this series on silica mobility in evaporitic settings focused on the most mobile (soluble) form of silica known as opal-A or amorphous silica which is defined by a broad peak in XRD determinations (Figure 1). Based on that discussion, it seems there are three main ways modern amorphous silica precipitates; 1) Inorganic precipitate (as in the crusts of the Coorong ephemeral lakes, 2) As a replacement of sodium silicates, such as magadiite (as in alkaline lakes in the African Rift Valley, and 3) Biogenically as in diatom and radiolarian tests in various lakes and the oceans. In all three Opal-A (amorphous opal) is the dominant form of SiO_2, but there are other more crystalline forms of sedimentary silica Quaternary sedimentary settings with additional opaline and more quartzose forms. Knauth (1994) classified authigenic silica into, a) 3 types of amorphous opal (opal-A, opal-CT, and opal-C) and, b) 5 types of quartz (granular microcrystalline quartz, megaquartz, length-fast chalcedony, length-slow chalcedony, and zebraic chalcedony).

Unlike quartz, the opaline minerals are metastable and show different degrees of crystallinity, crystal structure and proportions of water. Jones and Segnit (1971) classified opal minerals into three groups, according to their X-ray diffraction (XRD) patterns (Figure 1a): Opal A (with an XRD pattern that resembles that of amorphous silica), Opal C (which shows four moderately broad peaks that coincide closely with the position of the four most intense peaks of α-cristobalite, plus minor evidence of α-tridymite), and Opal CT (with patterns that show signs of both α-cristobalite and α-tridymite). Opal A can be inorganic, but worldwide is frequently found as siliceous microfossils (diatom frustules, sponge spicules, phytoliths, etc.). Opal C is very rare in sediments. Opal-CT is the most common phase, but its structure can differ owing to its variable water content, the ratio of interlayered cristobalite/tridymite to the amorphous background, and the degree of stacking disorder within the silica framework (Guthrie et al., 1995).

So, amorphous silica is composed of relatively pure SiO_2 but with only very local crystallographic order. Amorphous silica includes various kinds of hydrated and dehydrated silica gels, silica glass,

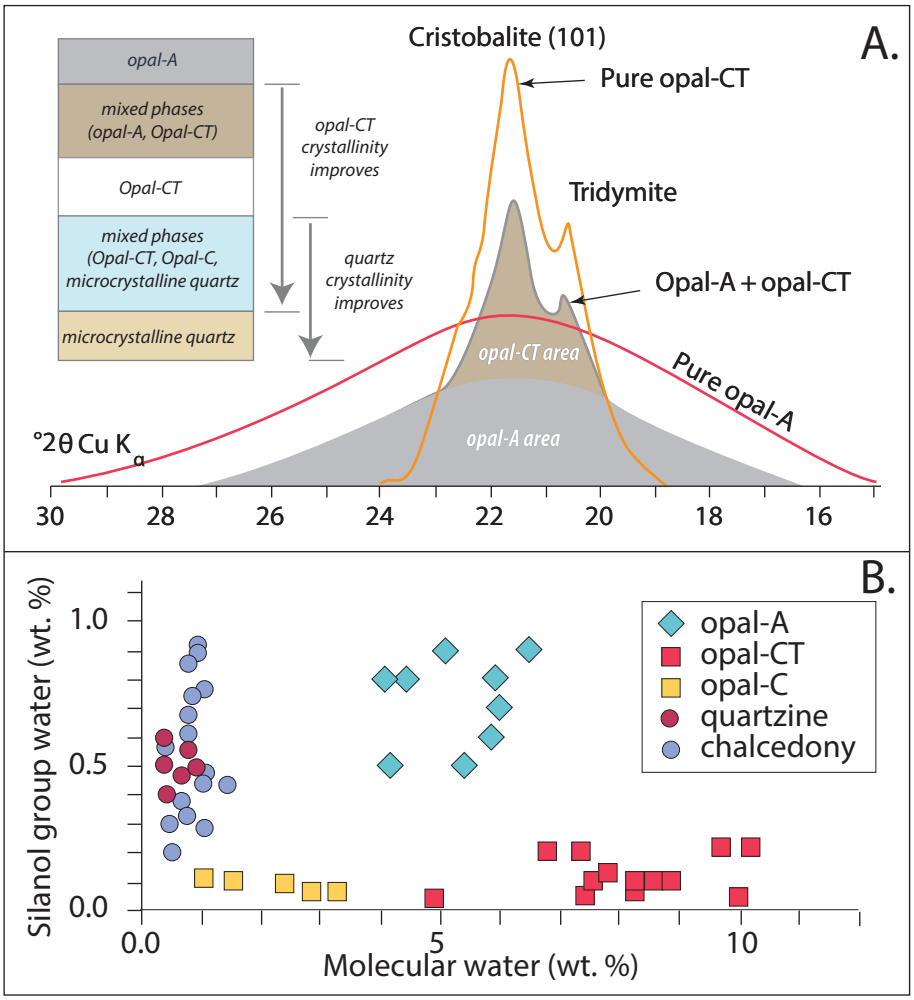

Figure 1. Silica rock properties A) XRD-based separation of different types of opaline silica. B) Water content of different forms of silica rocks

siliceous sinter formed in hot springs, and the skeletal materials of silica-secreting organisms. Opal or opaline silica is a solid form of amorphous silica with some included water (Figure 1b). It's abundant in young cherts, extending back into the Mesozoic. Its geological occurrence is varied it can be by alteration of volcanic ash, precipitation from hot springs, and, volumetrically most significant in the Phanerozoic via precipitation as skeletal material by certain silica-secreting organisms. Opal starts out as what is called opal-A, which shows only a very weak x-ray diffraction pattern, indicating that any crystallographic order is very local. With burial, during the initial stage of diagenesis, opal-A is transformed into opal-CT, which shows a weak x-ray diffraction pattern characteristic of cristobalite). Upon further diagenesis, opal-CT is transformed into crystalline quartz, resulting in chert that consists of an equant mosaic of microquartz crystals. Chalcedony is made up of needles or fibers, often spherulitic, composed of quartz. There's probably amorphous silica in among the needles, and a variable water content. It is metastable with respect to ordinarily crystalline quartz, but it persists across long time frames; it's found even in some Paleozoic cherts. Porcellanite is the porous form of chert while silicilyte is a related form that typifies evaporite-associated bacterially-mediated sediment forming a producing reservoir in the South Oman Salt Basin (later blog).

During burial diagenesis, opaline phases age by undergoing successive dissolution-precipitation-recrystallization reactions including the well-known opal A-opal to CT to quartz transition (Williams and Crerar, 1985; Williams et al., 1985). These transformations depend mainly on time and temperature, but accelerate in meteoric diagenetic settings, where quartz crystals can form directly, and bypass the opaline silica polymorph phase (Arakel et al., 1989; Bustillo and Alonso-Zarza, 2007). The existence of opal-CT in very young and at-surface rocks (Jones and Renaut, 2007; Jones et al., 1996) shows that time is not necessarily "a cause" in silica diagenesis. According to Bustillo (2010) in continental environments, very rapid silica alteration appears to be related to efficient fluid delivery (i.e., hydrogeology), as much as to time.

When opal-A or opal-CT occur in a sedimentary host, their ageing sets silica free in a dissolved form and so influences the diagenetic evolution of the adjacent carbonates, generally producing silica/carbonate replacements, silica cement, or neoformed silicate clay. Quartz is the last stage of the recrystallization of opals, but can also form directly via replacement or the cementation of voids. Such quartz shows many textures under polarising light. Common quartz can have different crystal sizes and forms crypto-, micro-, meso- or macrocrystalline mosaics. Maliva and Siever (1988) indicated that meso- and macrocrystalline quartz are not produced by ageing but only by direct precipitation during replacement or cementation. Chalcedony is a fibrous-texture quartz made up of several different varieties classified by the orientation of the fibres with respect to the crystal's c-axis, namely (Figure 2a): Calcedonite (length-fast chalcedony, in which the elongation of the fibres is perpendicular to the crystallographic c-axis), quartzine (length-slow chalcedony, in which the elongation is parallel), lutecite (another type of length-slow chalcedony, in which the fibre axis is inclined by approximately 30°), and helicoidal calcedonite or zebraic chalcedony (which shows a systematic helical twisting of the fibre axes around the crystallographic c-axis). These varieties of chalcedony allow the identification of the environment reigning during the replacement or cementation as acid or non-sulphate (length-fast), or basic or sulphate/magnesium-rich (length-slow) (Figure 2; Folk and Pittman, 1971). The host material, therefore, has geochemical control over the textures of quartz precipitated. Unfortunately, there are exceptions to these rules, and the strict application of

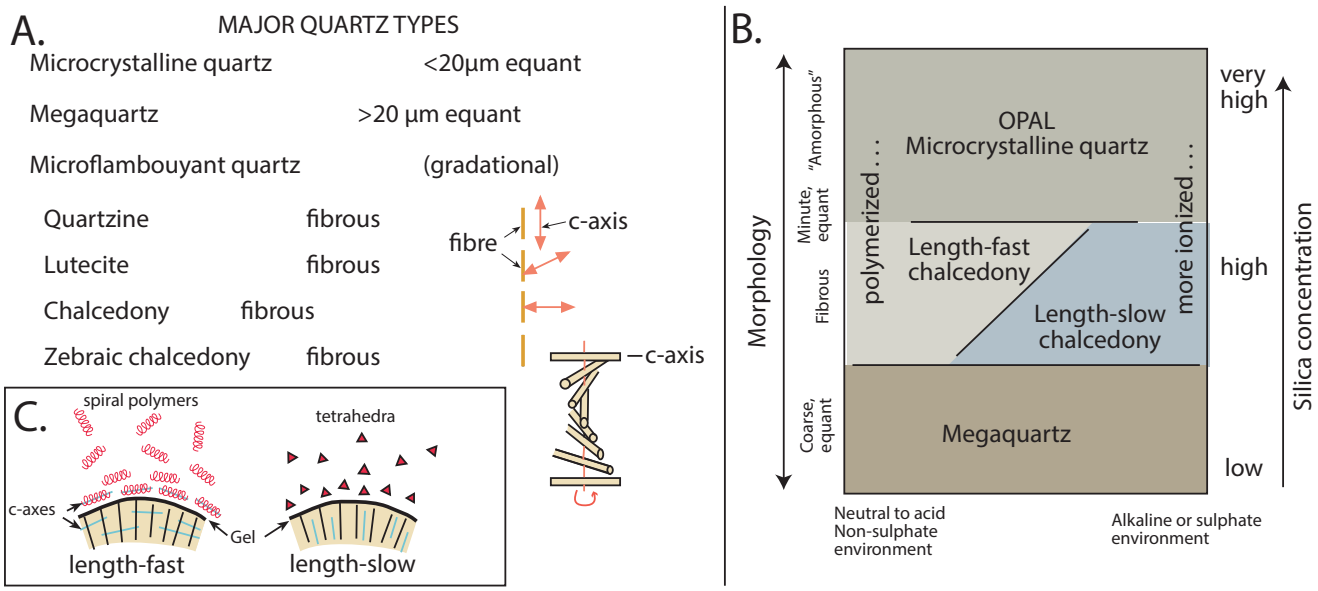

Figure 2. Chalcedony as an indicator of vanished evaporites. A) Major quartz types based on crystal size and orientation of chalcedony fibres with respect to c-axis (after Milliken, 1979). B) Style of chalcedony precipitate is controlled by the degree of polymerization, which in term reflects environment of precipitation. C) Crystallite orientation (single tetrahedra versus spiral polymers) with respect to growth surface controls formation of length slow versus length fast crystals - see text (B and C after Folk and Pittman, 1971).

these criteria can lead to errors of interpretation.

Moganite is a metastable monoclinic silica polymorph that is structurally similar to quartz (Miehe and Graetsch, 1992). The identification of moganite in the presence of quartz is difficult. It can be detected, however, by detailed XRD analyses with Rietveld refinements, and by other techniques such as Raman and NMR analysis. This mineral is found mixed with quartz in many cherts, preferentially in those that developed in evaporitic environments. However, it can also be produced by the replacement of biogenic carbonates during the interaction of the latter with groundwater (Heaney, 1995). Moganite transforms into quartz, as do the opaline phases, and it probably does so quite readily (Rodgers and Cressey, 2001).

In addition to its replacement style, a number of studies have investigated oxygen isotopic compositions ($\delta^{18}O$) in chert to infer climate-driven temperature change through time (Degens and Epstein 1962; Knauth and Epstein 1976; Knauth and Lowe 2003).

Silicification of calcium sulphate nodules and isolated crystals

Silicified anhydrite nodules and CaSO4 crystals are widely reported and reliably documented in sediments as old as Paleoproterozoic and as young as Holocene (Table 1). Quartzine and lutecite (aka length-slow chalcedony) typically infill or replace nodules that preserve characteristic cauliflower shapes of the antecedent anhydrite/gypsum nodule (Figure 3; Arbey, 1980; Hesse, 1989). According to Folk and Pittman (1971), rates of nucleation and crystallisation are the primary controls on crystal size and variety of silica precipitating in a void in a dissolving nodule. Rates, in turn, depend on the level of silica saturation or its concentration in the mother brine (Figure 2b, c). According to Keene (1983), precipitation of length-slow quartz is favoured in waters with high SO_4 and Mg levels.

High pH levels (alkaline conditions) in the mother solution tend to ionise dissolved silica. Neutral or low pH levels favour silica crystallites made up of combined $Si(OH)_4$ groups. These tend to polymerise into spiral chains at lower pH and higher concentrations. At high concentrations and high pH, the silica precipitates possess a fibrous chalcedonic form reflecting their rapid rates of precipitation. High pH at the precipitation site means silica crystallites also tends to be present in solution as single ionised tetrahedra that attach themselves one by one to the growing surface, so creating fibres of quartz with the c axes oriented parallel to the long axis of the growing fibres (length-slow). Under low pH or in non-sulphate settings the silica is polymerised into spiral silica chains that attach tangentially to the growth surface of the silica gel, with their c-axes parallel to the growing crystal surface and perpendicular to the future direction of the fibres (Figure 2c; length-fast; Folk and Pittman, 1971).

Milliken (1979) summarised the typical petrographic and hand specimen scale features of silica that replaced $CaSO_4$ nodules in Mississippian sediments of southern Kentucky and northern Tennessee (Figure 4). Such nodules typically have knobbly irregular cauliflower-like surfaces, while internal diagnostic textures include: 1) length-slow chalcedony after lathlike evaporites, especially anhydrite; 2) quartzine; and 3) small amounts of lutecite associated either with megaquartz that shows strong undulose extinction, or with euhedral megaquartz (Chowns and Elkins, 1974). The megaquartz often encloses small blebs of residual anhydrite.

Occurrence and age of host	Comments	Reference
Silica precipitates in Holocene alkaline lakes along the Coorong coastal plain, South Australia. Type area for "Coorong style" chert.	Direct precipitation (?bacterially mediated) of opal-cristobalite in small mm-scale vugs in and on the surface of tepee-overprinted strandzone magnesite/dolomite crusts around the edge of Milne Lake and probably in crusts in other lakes accumulating evaporitic lacustrine dolomite, magnesite, hydromagnesite, aragonite and gypsum.	Peterson and von der Borch (1965)
Nodules and polygons of chert in diatomaceous beds of the late Pleistocene High Magadi beds, Lake Magadi, Africa. Type area for "Magadi-style" chert.	Chert in nodules and polygons is a weathering product of sodium silicate gels. Conversion involves shrinkage and induration. It creates a characteristic "crocodile-skin" texture on the surface of newly formed chert. This texture is associated with soft sediment deformation in the surrounds and sodium carbonate salts in adjacent sediments.	Eugster, 1967; Jones et al., 1967; Hay, 1968
Pleistocene nodules in saline mudflats, Lake Olduvai, Africa.	Magadi-style chert nodules (crocodile-skin) formed by replacement of a sodium silicate (magadiite) precursor.	Hay and Kaiser, 2001
Double-terminated euhedral quartz in Pleistocene sabkha dolomite, offshore Al Jabyl, Saudi Arabia (Pleistocene "Herikimer diamonds").	Megaquartz as individual crystals and clusters of crystals and overgrowths on detrital quartz. Individual crystals up to 1 mm long, many with shallow dolomite mould impressions on their crystal faces, some partly, or completely, engulf dolomite rhombohedra.	Chafetz and Zhang, 1998
Gypsum-rich silica nodules, Moghra Formation, Miocene, Northwest Qattara depression, Western Desert, Egypt	Nodules occur in two shale horizons, consist mainly of quartz and are composed of gypsum-free matrix and gypsum-rich megacrystalline quartz. The matrix consists of microflamboyant quartz (less than 36 µm in diameter) and chalcedony. The megacrystalline quartz occurs as lenticular and prismatic forms (length: 90–250 µm; width: 30–90 µm). Structure of the silica nodules begins with quartzine in its outer rim, then gypsum-free microcrystalline quartz in the middle part and ends with gypsum-rich lenticular to prismatic megaquartz in the nodule center.	Khoriby et al., 2005
Chert nodules in gypsiferous limestones of the Kef Eddour Member (Ypressian-Priabonian- Eocene) near Metlaoui and Sehib (Tunisia)	Silica with $\delta^{18}O$ values from +25 to +28.6% (SMOW)]replaced the outer parts of anhydrite nodules at pH < 9. In contrast, pore-fluid pH values > 9 in the innermost parts of the anhydrite nodules prevented silica precipitation. This chemical barrier is preserved in the microquartz rims left after dissolution of the remaining anhydrite.	Henchiri and Slim-S'Himi, 2006
Quartz geodes and nodular chert in Campanian (Cret.) marly clays and calcarenites, Basque-Cantabrian Basin, Northern Spain.	Silica replacement of cauliflower geodes and chert as spherulitic fibrous quartz (quartzine-lutecite). There are small anhydrite laths included in some of the megaquartz crystal fills.	Gomez-Allday et al., 2002
Quartz geodes and chert hosted in Triassic red mudstones, Bristol district of the UK.	Silica replacement in open voids after cauliflower textured anhydrite. Loose euhedral double-terminated quarts crystals aggregating on bottom of some geodes after the $CaSO_4$ is dissolved and are called "Bristol Diamonds."	Tucker, 1976a
Nodules developed in a single layer in Bundsandstein (Triassic) redbeds, Iberian Range, Central Spain.	Cauliflower shaped chert nodules and geodes, some are filled with concentric layers of quartz and carbonate, others are still open and partially filled and fractured. Relict anhydrite textures and rare laths, bacteria played a role in dolomitisation of some nodules.	Alonsa-Zarza et al., 2002
Chert nodules in Triassic of North Carolina, USA.	Cauliflower chert with relict anhydrite.	Wheeler and Textoris, 1978
Nodules and crystals in Lower Purbeck Beds, (Jurassic) Dorset, UK.	Silica replacement of individual and clustered gypsum bird-beaks and enterolithic anhydrite nodules (with small relics of anhydrite preserved).	West, 1964; 1973
Discrete horizons, scattered nodules in layers and individual replaced crystals in Seven Rivers, Yates and Tansill formations, Guadalupe Mountains, (Permian) Delaware Basin, USA.	Cauliflower nodule and geodes. Nodules, bird-beak gypsum, axehead anhydrite were all replaced by silica and calcite spar. Initial replacement by black megaquartz (with anhydrite, dolomite, water and hydrocarbon inclusions). This was followed by blocky calcite spar fill of voids created by late-stage dissolution of remaining anhydrite (telogenetic).	Ulmer-Scholle et al., 1993
Thin layers of chert nodules in fluvio-lacustrine muds sandwiched in acidic volcanics of the Lower Permian Bolzano Volcanic Complex, Northern Italy.	Magadi-style chert showing soft-sediment deformation and shrinkage cracks (crocodile-skin), imply a sodium silicate parentage. Transformation to quartz and concomitant (re)crystallization created a variety of silica textures, dominated by microflamboyant quartz.	Krainer and Spötl, 1998
Fist-sized nodules and geodes in layers and dispersed zones in Fort Payne Fm., Warsaw Limestone, St Louis Limestone (Mississippian) of south-central Kentucky and Tennessee, USA.	Concludes that megaquartz characterized by strong undulose, radial extinction, the existence of anhydrite laths included in megaquartz crystals with 'cubic' appearance terminations, the growth of spherulitic, fibrous-radial quartz aggregates (quartzine-lutecite), and crusts of zebraic chalcedony are all evidence of silica replacing anhydrite nodules.	Milliken, 1979
Fist-sized nodules and layers in Fort Payne Fm. and Warsaw Limestone, (Mississippian) near Woodbury, Tennessee, USA.	Silica replacement of anhydrite to form cauliflower cherts with outlines reminiscent of the nodules in the Abu Dhabi sabkha. Soft sediment deformation in the surrounding matrix argues silicification took place prior to complete induration of matrix. Silica was derived from sponge spicules.	Chowns and Elkins, 1974
Silicified nodules and clasts representing anhydrite pseudomorphs in Mississippian Wexford Fm., Ireland.	Evaporites indicators mostly as chert nodules and clasts representing pseudomorphs of former now silicified gypsum within the breccia unit and also as distinct anhydrite/gypsum beds, over 2m thick, within the breccia and as rare gypsum veins.	Nagy et al., 2005
Silicified anhydrite nodules, Pimenta Bueno Formation, Siluro-Devonian in the Parecis Basin, central Brazil.	The playa-lake deposits show early diagenetic dolomitisation of lime mud, precipitation of anhydrite nodules and extensive silicification. Theses anhydrite nodules were replaced by gypsum and chalcedony during telodiagenesis.	Goldberg et al., 2011
Pseudomorphs after anhydrite in the Mines Subgroup (Neoproterozoic), in the Katangan Copperbelt, Democratic Republic of Congo.	Silicified anhydrite defines oval, round and cauliflower-shaped nodules, or in lenses that may be wedge-shaped, or as laths. There are two main types of siliceous replacement and cementation. Type 1: dolomite precipitated first and was replaced by Cu–Co sulphides and authigenic quartz. Relicts of anhydrite and halite are still present. Type 2, authigenic quartz and sulphides precipitated prior to dolomite and the crystals are free growing	Muchez at al., 2008
Palaeoproterozoic chert nodules in the Bartle Member (2.2 Ga) of the Killara Formation, Yerrida Group, Yerrida Basin of Western Australia	Association indicates an evaporitic-pyroclastic-thermal-spring environment associated with rifting at about 2.2 Ga. The chert member contains silica pseudomorphs after evaporite minerals that in places enclose relict isolated crystals and aggregates of crystals of gypsum and anhydrite. The evaporite minerals are associated with minerals such as baryte and analcime	Pirajno and Grey, 2002

Table 1.

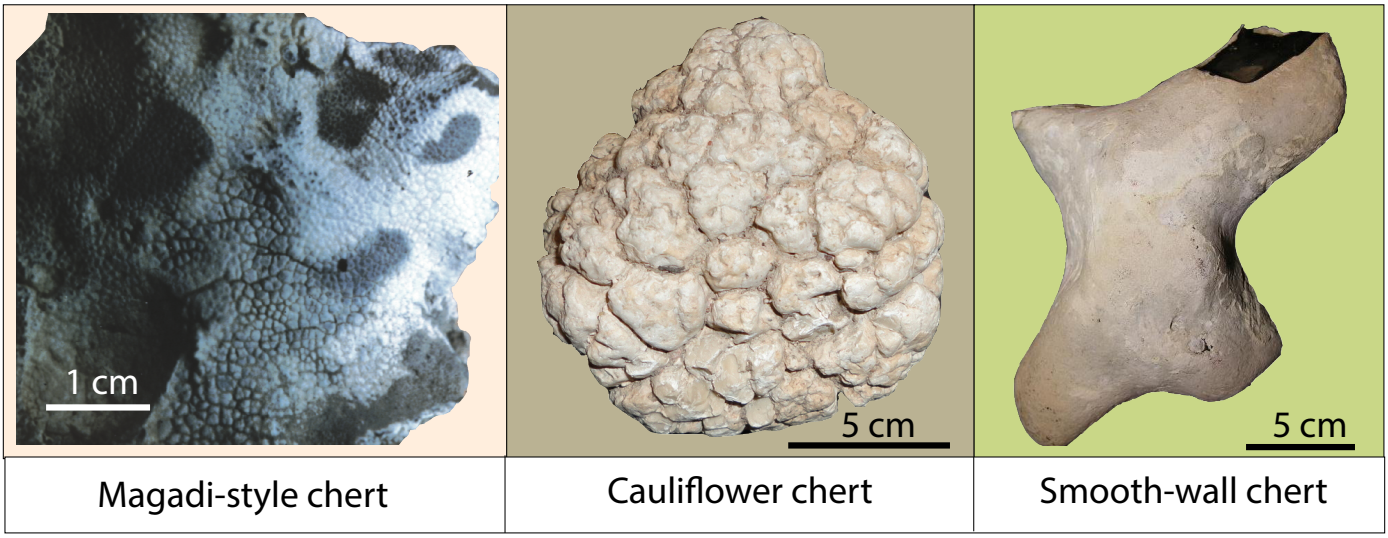

Figure 3. Surface textures of the three main styles of chert nodules. Magadi-style cherts show characteristic reticulate shrinkage features on nodules and likely form via silicification of a sodium silicate precursor. Cauliflower cherts indicate silicification and replacement of a former anhydrite nodule , which formed via coalescence of smaller anhydrite nodules. Smooth-walled chert nodules are typical marine diagenetic features in biogenic ocean sediments

Many buried calcium sulphate nodules are silicified in a multistage process that involves both replacement and void filling (West, 1964; Chowns and Elkins, 1974). The process commences about the margins of a nodule (stage 1) with a volume for volume replacement of anhydrite by microcrystalline quartz. It generally ends with the growth of euhedral drusy quartz crystals into a central vug (stage 2 and 3). This mode of replacement exemplifies textural changes as seen from the edge toward the centre of the geode in texture style A in Figure 4. However, as noted by Milliken (1979) this edge inward evolution of the geode or nodule fill is typified by a variety of textural styles, which she denoted a styles A through D.

Stage 1 chalcedony or quartzine mimics or pseudomorphs the felted lath textures of the precursor anhydrite in the outer portion of the nodules in all styles. Anhydrite pseudomorphs occur as radiating or decussate aggregates with a distinctive flow-like pattern indicating a felted anhydrite precursor. Identical decussate and flow textures occur in laths that make up sabkha anhydrite nodules and defines their explosive mode of growth, as well as the typical coalesced nodule texture that, when replaced, ultimately controls the broad-scale "cauliflower" outline of the whole replaced nodule (Figures 3 and 5). And so, as well as silicified lath microtextures seen in thin section, outlines of larger crystals that predated anhydritisation and silicification may be preserved by the nodule margin, these crystal outlines vary from prismatic to bladed. Many silicified nodules still retain the knobbly cauliflower surface morphology of its precursor anhydrite; other nodule edges preserve crystal pseudomorphs with the interfacial outlines of gypsum or anhydrite precursors.

Stage 2 microquartz and quartz fill can assume euhedral faces as they grow into voids created by the dissolution of the nodule. At the same time the quartz may continue to engulf and pseudo-

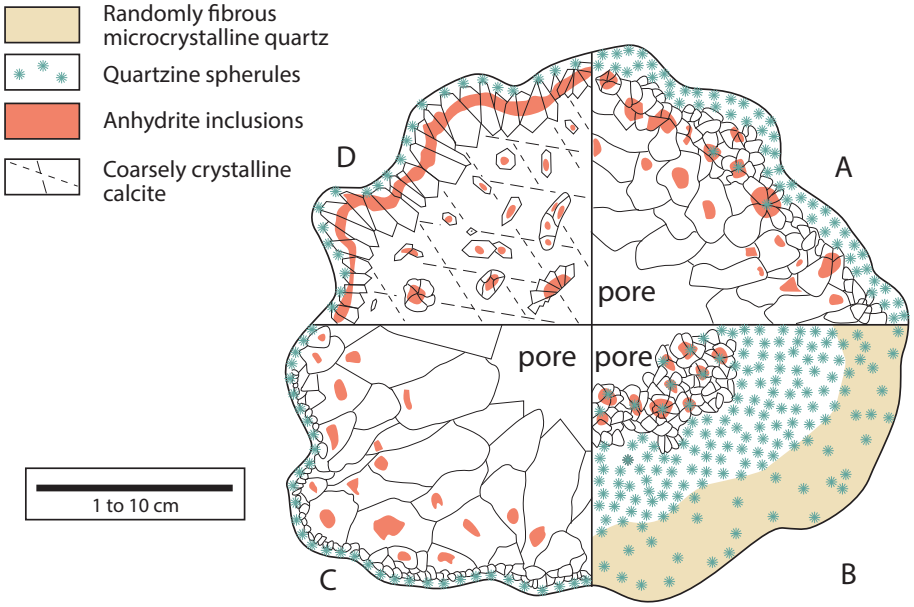

Figure 4. Texture in silicified-calcitized anhydrite nodules (cauliflower chert). A) Most common style of nodule with thin rim of spherulitic quartzine followed inward by megaquartz characterised by increasing crystal size and with frequent anhydrite inclusions. B) Nodule with a large proportion of fibrous quartz. Thick rim of spherulitic quartz passes inward to strongly undulose megaquartz. Some of the megaquartz has anhydritic nuclei. C) Nodule with a thin rim of spherulitic quartzine passing inward to a large proportion of megaquartz. D) Nodule with megaquartz rim and an interior filled with calcite. Calcite may have filled a cavity or replaced earlier silica. Late stage cavity-fill calcite is often defined by a thin rim of authigenic baryte or sulphide, prior to precipitation (modified from Milliken, 1979).

morph small areas of residual anhydrite or other less common evaporite salts (e.g. styles A, C, D). Quartz crystals precipitated at this stage are commonly zoned, with more anhydrite inclusions found within the inner region of the pseudomorph. Some quartz crystals are doubly terminated and probably grew via the support of a dissolving meshwork of anhydrite. With the final dissolution of the supporting mesh, these quartz crystals sometimes dropped to the floor of the void to create a geopetal indicator. For example, such highly birefringent anhydrite spots define cauliflower nodules in 2.2 Ga sediments in the Yerrida Basin, Australia (El Tabakh et al., 1999).

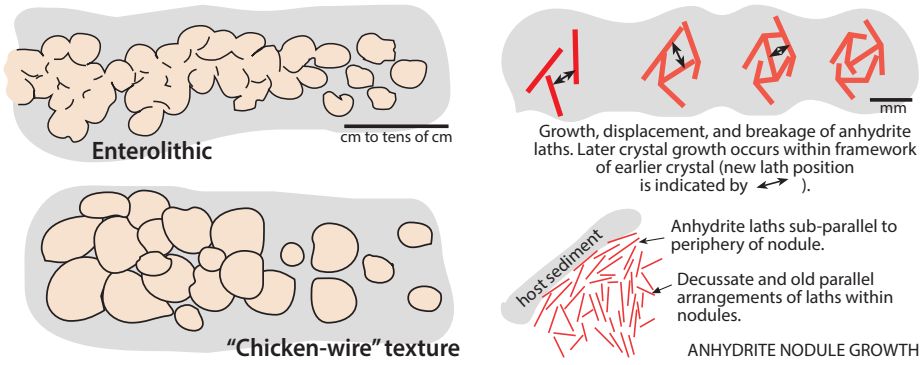

Figure 5. Anhydrite nodule growth as smaller nodules grow and coalesce in a larger structure with a boundary resembling the coalesced florets in a cauliflower. The nodules tend to coalesce into chicken wire and enterolithic anhydrite structures. Finer detail on right hand size of diagram shows how successive new anhydrite laths break and rotate earlier formed laths in an expanding nodule. The end result is a nodule with a margin composed of laths aligned subparallel to the its edge. Many nodule interiors preserve clusters of subparallel laths showing large nodules grow by accretion of smaller nodules (after Shearman and Fuller, 1969; Warren 2016).

Stage 3, the final stage of the void fill is typified by the precipitation of coarse drusy euhedral quartz with no included anhydrite. This coarse quartz resembles coarse vein quartz and often has ^{18}O values indicating temperatures of the mesogenetic or burial realm.

Sometimes the processes of void fill may be arrested to leave a hollow core in the silica-lined geode (Styles A, B, C). The void may be filled later by a different burial stage cement such as baryte, sparry carbonate (e.g. ferroan dolomite or calcite), or even metal sulphides. This is the case with the large (up to 1 m diameter) silicified cauliflower-shaped anhydrite nodules of Proterozoic Malapunyah Formation of the McArthur Basin in Northern Australia where baryte, then metal sulphides and then sparry calcite typify the latter stages of void fill (pers. obs.). Similar fracture-filling baryte characterises the later diagenetic stages of silicified and calcitised anhydrite nodules in the Triassic Bundsandstein redbeds of the Iberian Range of central Spain (Figure 6; Alonso-Zarza et al., 2002). Such geodes are typically excellent indicators of burial cement stratigraphy in a mudstone matrix that otherwise preserves few signs of the evolving pore fluid chemistry. Thus textures and isotopic signatures in a replaced nodule can indicate ongoing diagenesis of the anhydrite nodule that preserves aspects of the shallow active phreatic (eogenetic), the mesogenetic zone with basinal brines and then uplift-related telogenetic fluids.

Internally, cauliflower chert may retain no evidence of former anhydrite lathes mimicked in chalcedony, but can be filled with various styles of coarser-grained megaquartz. The resulting nodules still retain the outline of the precursor evaporite nodule (Figure 3). Work on diagenetic timing of numerous silicified CaSO4 nodules (e.g. Milliken, 1979; Geeslin and Chafetz, 1982; Gao and Land, 1991; Ulmer-Scholle and Scholle, 1994) shows that most silica replacement begins with shallow burial, either in the zone of active phreatic flow or in the upper portion of the zone of compactional flow (probably at depths of less than 500-1000 m). Early silica replacement in the zone of active phreatic flow is indicated by a lack of compressional flattening of the nodule, by the preservation of delicate surface ornamentation and the preservation of compactional drapes around replaced nodules. If replacement of an anhydrite nodule occurs later in the burial cycle, the anhydrite nodule has by then become flattened or sluggy and no longer retain a rugose surface. The result can be a series of "cucumbers" rather than "cauliflowers."

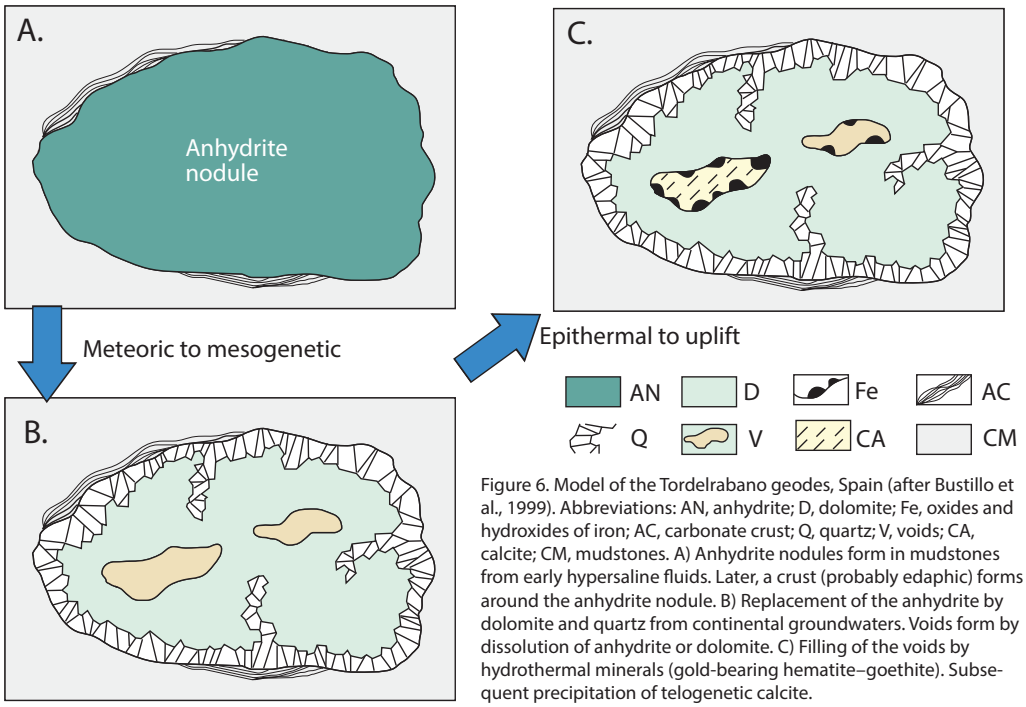

Figure 6. Model of the Tordelrabano geodes, Spain (after Bustillo et al., 1999). Abbreviations: AN, anhydrite; D, dolomite; Fe, oxides and hydroxides of iron; AC, carbonate crust; Q, quartz; V, voids; CA, calcite; CM, mudstones. A) Anhydrite nodules form in mudstones from early hypersaline fluids. Later, a crust (probably edaphic) forms around the anhydrite nodule. B) Replacement of the anhydrite by dolomite and quartz from continental groundwaters. Voids form by dissolution of anhydrite or dolomite. C) Filling of the voids by hydrothermal minerals (gold-bearing hematite–goethite). Subsequent precipitation of telogenetic calcite.

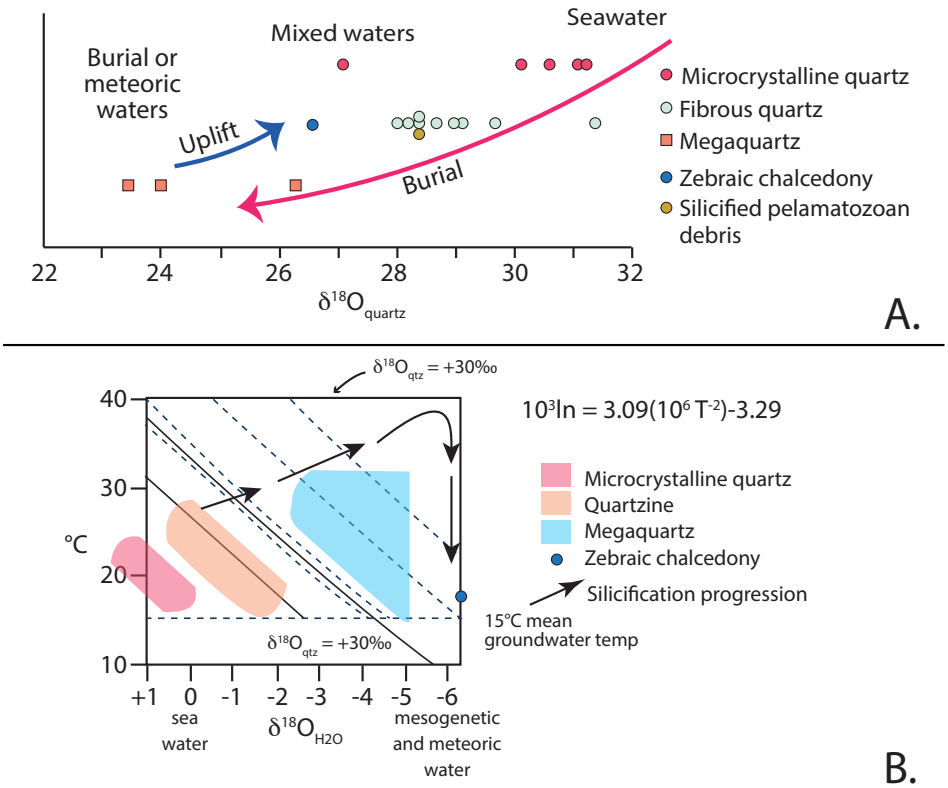

Figure 7. Isotope values in nodule burial and replacement. A) Correlation of quartz types with $\delta^{18}O$ values and the interpreted silicification history. B) Spectrum of temperature and $\delta^{18}O$ values possible according to the equation of Knauth and Epstein (1976). Diagonal lines are $\delta^{18}O_{qtz}$ values values. Solid diagonals are for reference. Dashed diagonals represent the high and low $\delta^{18}O_{qtz}$ values for the quartz types indicated. Shaded areas represented interpreted conditions of formation of the different quartz types (after Milliken, 1979).

Milliken's (1979) isotopic evidence implies much silica replacement in the nodules she studied was relatively early in the burial cycle at temperatures that were < 40°C. Silica was supplied by through flushing pore fluids with compositions ranging from seawater to mixed meteoric-seawater. Of course, nodule replacement by silica or calcite does not have to happen on the way down in the burial cycle; it may also happen during uplift back into the telogenetic realm, where the strata have once again entered the zone of active phreatic flow (Figure 7).

Until the turn of the century, there were no documented examples of the process of evaporite replacement by quartz in Quaternary sediments. Now, autochthonous, doubly-terminated, euhedral megaquartz crystals have been observed infilling voids in a gypsum- and anhydrite-bearing Pleistocene sabkha dolomite sequence in the Arabian Gulf, as well as forming overgrowths on detrital quartz grains (Chafetz and Zhang, 1998). These siliceous sabkha precipitates are forming within metres of the present sediment surface with a silica source that is probably recycled biogenic material. Individual quartz crystals attain lengths of 1 mm. Many quartz crystals faces preserve impressions of dolomite rhombs or they partly, or entirely, engulf dolomite rhombohedra. This process of replacement is a response to changing fluid chemistry tied early phreatic burial, to see the full suite of silica replacement textures and the variations in the timing of the replacement means one must study ancient evaporite sequences (Table 1).

Overall, the texture of silica infill or replacement in a $CaSO_4$ nodule is dependent on the rate of sulphate dissolution, the timing of silica precipitation and the rate of silica supply. Some nodules are dominated by the early lit-par-lit replacement textures (styles A and C in Figure 4), others have textures indicating silica cement (aligned megaquartz)

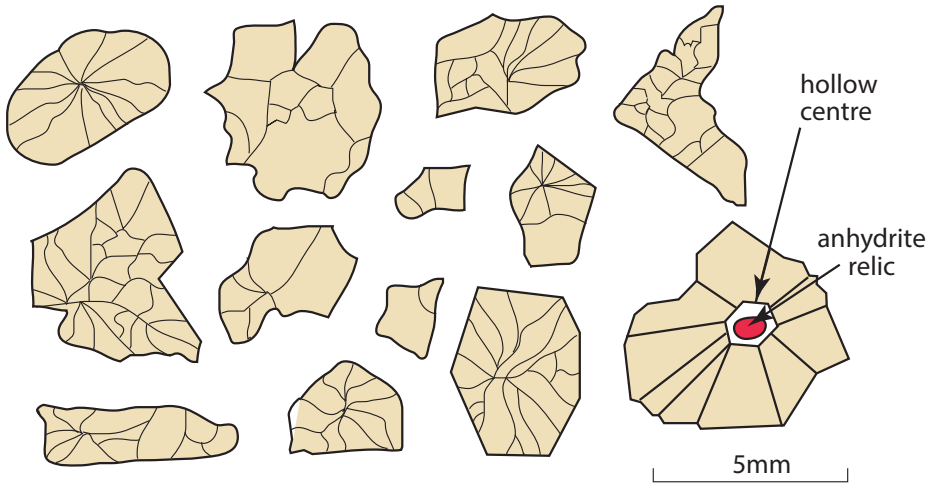

Figure 8. Sketches showing various shapes of the quartz nodules and internal arrangements of megaquartz crystals from replaced anhydrite nodules in the Mesoproterozoic Wollogorang Formation of northern Australia and the Neoproterozoic Gaissa Sandstone/Porsanger Dolomite of Finnmark, Arctic Norway (in part modified from Tucker, 1976b).

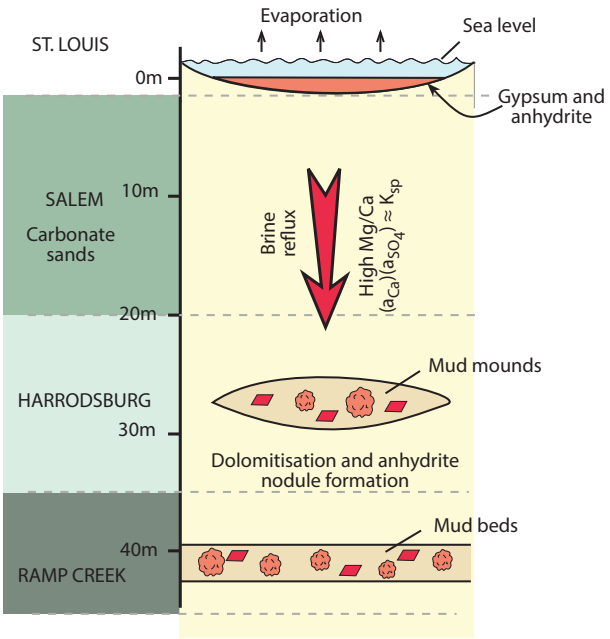

Figure 9. Precipitation of anhydrite and gypsum during St. Louis Limestone deposition formed a dense magnesium- and sulphate-rich brine that percolated downward and seaward through the then unlithified sands of the Salem Limestone. Dolomitisation of carbonate mud mounds and beds in the Harrodsburg and Ramp Creek Formations released calcium causing pore waters to become supersaturated with respect to anhydrite, resulting in the precipitation of anhydrite nodules that were later silicified (after Maliva, 1987).

growing into an open phreatic void left after the complete dissolution of the $CaSO_4$. Such nodules may still retain a hollow centre where the anhydrite once resided (Figure 8). When a silica-filled geode did not start to accumulate silica until after all the $CaSO_4$ dissolved, the primary evidence for an evaporite precursor comes from the shape of the replaced nodule and its stratigraphic position within the evaporitic depositional sequence, e.g. beneath an erosional surface that defines the top of the capillary zone.

Not all the anhydrite nodules, now replaced by silica, were syndepositional. Maliva (1987) showed that nodular anhydrite parent, now indicated by quartz geodes in the Sanders Group of Indiana, first precipitated in the subsurface, while its surrounding matrix of normal-marine Sanders Group sediment was still unlithified (Figure 9). Anhydrite nodules formed in the subsurface during early burial as hypersaline reflux brines sank into the normal-marine limestones of the Ramp Creek and Harrodsburg Formations. Silica subsequently replaced the anhydrite nodules. These geodes are almost invariably associated with the development of reflux dolomite.

Similarly, not all silica-replacing anhydrite in a particular region need come from the same source or be emplaced by the same set of processes. Silicified nodules within middle-upper Campanian (Cretaceous) carbonate sediments from the Lafio and Tubilla del Agua sections of the Basque-Cantabrian Basin, northern Spain preserve cauliflower morphologies, together with anhydrite laths enclosed in megaquartz crystals and spherulitic fibrous quartz (quartzine-lutecite). All this shows that they formed by ongoing silica replacement of nodular anhydrite (Figure 10; Gómez-Alday et al., 2002). Anhydrite nodules at Lafio were produced by the percolation of saline marine brines, during a period corresponding to a depositional hiatus. They have $\delta^{34}S$ and $\delta^{18}O$ mean values of +18.8‰ and +13.6‰ respectively, consistent with Upper Cretaceous seawater sulphate values. Higher $\delta^{34}S$ and $\delta^{18}O$ (mean values of + 21.2‰ and 21.8‰, respectively) characterise nodules in the Tubilla del Agua section and are interpreted as indicating a partial bacterial sulphate reduction process in a more restricted marine environment (Figure 10a). Later calcite replacement and precipitation of geode-filling calcite in the siliceous nodules occurred in both sections, with $\delta^{13}C$ and $\delta^{18}O$ values indicating the participation of meteoric waters in both regions (Figure 10b). The synsedimentary activity of the Penacerrada diapir (Kueper salt - Triassic), which lies close to the Lafio section, played a significant role in driving the local shallowing of the basin and in the formation of the silica in the anhydrite nodules. In contrast, eustatic shallowing of the inner marine series in the Tubilla del Agua section led to the generation of morphologically similar quartz geodes, but from waters not influenced by brines derived from the groundwater halo of a diapir.

So far the various papers we have discussed relate the onset of

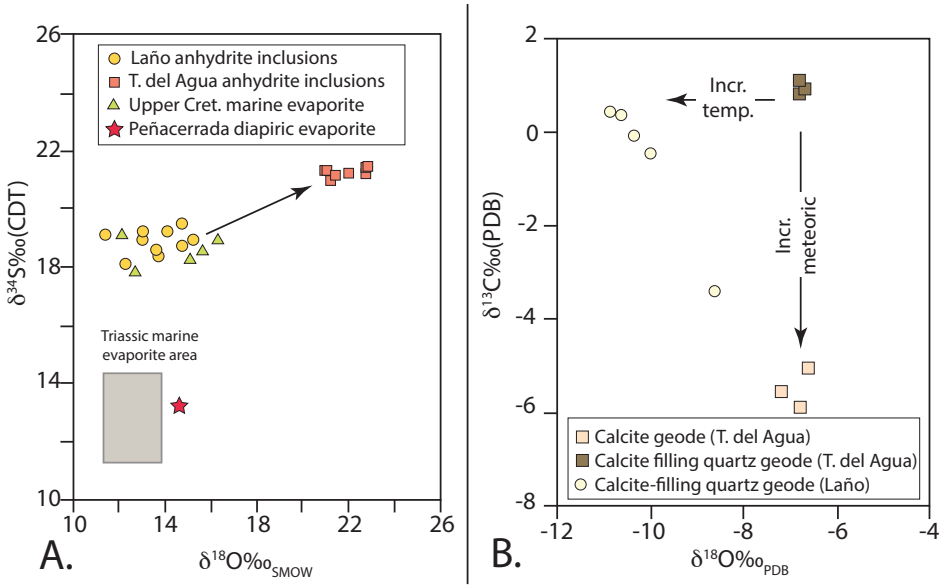

Figure 10. A) Plot of oxygen versus sulphur isotope composition of the Laño and Tubilla del Agua anhydrite inclusions in silicified nodules, together with other Triassic and Upper Cretaceous evaporite values from Spain. B) Oxygen versus carbon isotope composition of the Laño and Tubilla del Agua calcites. The Tubilla del Agua values define a vertical meteoric calcite line where the lighter ^{13}C values indicate the vadose zone while the higher values denote a phreatic zone. More negative ^{18}O values from the Laño section indicate an increase in temperature of the pore-waters.

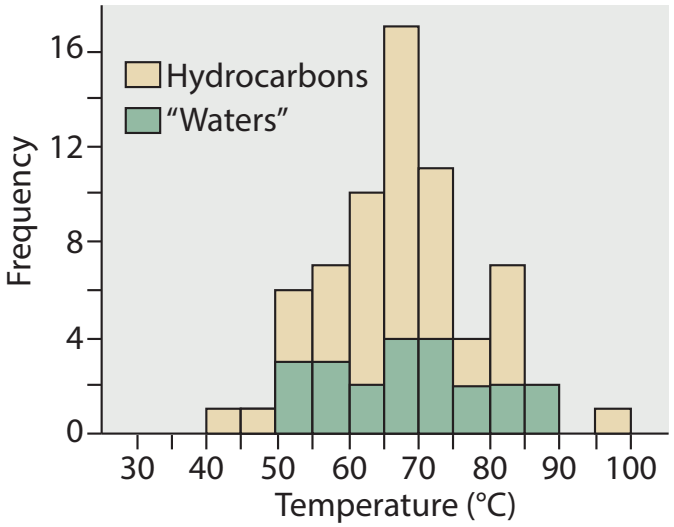

Figure 11. Plot of homogenization temperatures of both brine and hydrocarbon inclusions in replacement megaquartz in silicified sulphate nodules. Note the close agreement between the temperatures of the two phases. Average temperatures for the brine and hydrocarbon-filled inclusions are 67.1°C and 67.7°C, respectively (after Ulmer-Scholle et al., 1993)..

silicification to active phreatic hydrologies (brine reflux or meteoric) typically in evaporites in host rocks that are shallow, either in the early stages of burial or later in the uplift realm. In contrast in a paper discussing silicification of sulphate nodules in Permian (Guadalupian) back-reef carbonates of the Delaware Basin, Ulmer-Scholle et al., 1993, conclude these nodules were silicified in the Mesogenetic realm. Replacement occurred at temperatures of 60-90°C at the same time as hydrocarbons were moving with basinal brines through the adjacent porous matrix (Figure 11). Silicification of these evaporite nodules proceeded from the exterior to the interior of the nodules. The fluid inclusions in the replacive megaquartz are primary, and many contain both hydrocarbons and water. In this setting it seems evaporite silicification was coeval with or slightly postdated hydrocarbon migration and the silica was likely sourced by dissolution of siliciclastics in nearby back-reef units.

Birnbaum and Wireman (1985) argued that bacterial degradation of organic matter must be important in forming silica precipitates in most evaporites. They demonstrated, through experiment, the strong influence of bacterial sulphate reduction on silica solubility. The ability of sulphate-reducing bacteria to remove silica from solution is related to local changes in pH and hydrogen bonding within amorphous silica, followed by polymerization to higher weight molecules. During silica replacement of sulphate evaporites at relatively shallow burial depths, the pore fluid becomes depleted in dissolved sulphate as it is reduced to H_2S by the action of anaerobic sulphate-reducing bacteria, which metabolise sulphate from an anhydrite or gypsum substrate. Where this selective dissolution of the sulphate occurs in the presence of amorphous silica, the reaction is accompanied by the precipitation of silica. Hence the microscale mimicry of the lath outlines in the outer parts of many replaced nodules. According to Birnbaum and Wireman, it reflects bacterially-mediated silica replacement of nodules in relatively shallow burial settings where bacteria flourish.

In summary, in terms of processes and diagenetic settings associated with Phanerozoic evaporite silicification it seems abiological processes, including thermochemical sulphate reduction and hydrocarbon migration, are more important at greater burial depths where bacteria no longer survive. Providing matrix permeability is retained, silica replacement can continue into the thermobaric stage and if the sulphate nodule survives mesogenetic replacement can even persist into exhumation. Replacement under a thermobaric regime is frequently indicated by the preservation of hydrocarbon inclusions in the infilling silica cement. Both BSR and TSR will be discussed further in the next blog article, dealing with silicification associated with ancient evaporites, but with more emphasis on possible hydrochemical contrasts between the Precambrian and Phanerozoic subsurface waters.

References

Alonso-Zarza, A. M., Y. Sánchez-Moya, M. A. Bustillo, A. Sopeña, and A. Delgado, 2002, Silicification and dolomitization of anhydrite nodules in argillaceous terrestrial deposits: an example of meteoric-dominated diagenesis from the Triassic of central Spain: Sedimentology, v. 49, p. 303-317.

Arakel, A. V., G. Jacobson, M. Salehi, and C. M. Hill, 1989, Silicification of calcrete in paleodrainage basins of the Australian arid zone: Australian Journal of Earth Sciences, v. 36, p. 73-89.

Arbey, N., 1980, Les formes de la silice et l'identification des évaporites dans les formations silicifiés: Bulletin, Centre Recherche Exploration–Production Elf- Aquitaine, v. 4, p. 309-365.

Birnbaum, S. J., and J. W. Wireman, 1985, Sulfate-reducing bacteria and silica solubility; a possible mechanism for evaporite diagenesis and silica precipitation in banded iron formations: Canadian Journal of Earth Sciences, v. 22, p. 1904-1909.

Bustillo, M. A., 2010, Chapter 3 Silicification of Continental Carbonates, in A. M. Alonso-Zarza, and L. H. Tanner, eds., Developments in Sedimentology, v. Volume 62, Elsevier, p. 153-178.

Bustillo, M. A., and A. Alonso-Zarza, 2007, Overlapping of pedogenesis and meteoric diagenesis in distal alluvial and shallow lacustrine deposits in the Madrid Basin, Spain: Sedimentary Geology, v. 198, p. 255-271.

Chafetz, H. S., and J. L. Zhang, 1998, Authigenic euhedral megaquartz crystals in a Quaternary dolomite: Journal of Sedimentary Research Section A-Sedimentary Petrology & Processes, v. 68, p. 994-1000.

Chowns, T. M., and J. E. Elkins, 1974, The origin of quartz geodes and cauliflower cherts through the silicification of anhydrite nodules: Journal Sedimentary Petrology, v. 44, p. 885-903.

Clayton, C. J., 1986, The chemical environment of flint forma-

tion in Upper Cretaceous chalks, in G. d. G. Sieveking, and M. B. Hart, eds., The Scientific Study of Flint and Chert: Cambridge, Cambridge University Press, p. 43-54.

Degens, E. T., and S. Epstein, 1962, Relationship between O18/O16 ratios in coexisting carbonates, cherts, and diatomites: Bulletin American Association Petroleum Geologists, v. 46, p. 534-542.

El Khoriby, M., 2005, Origin of the gypsum-rich silica nodules, Moghra Formation, Northwest Qattara depression, Western Desert, Egypt: Sedimentary Geology, v. 177, p. 41-55.

El Tabakh, M., K. Grey, F. Pirajno, and B. C. Schreiber, 1999, Pseudomorphs after evaporitic minerals interbedded with 2.2 Ga stromatolites of the Yerrida basin, Western Australia: Origin and significance: Geology, v. 27, p. 871-874.

Eugster, H. P., 1967, Hydrous sodium silicate from Lake Magadi, Kenya: precursors of bedded chert: Science, v. 157, p. 1177-1180.

Folk, R. L., and J. S. Pittman, 1971, Length-slow chalcedony; a new testament for vanished evaporites: Journal Sedimentary Petrology, v. 41, p. 1045-1058.

Gao, G., and L. S. Land, 1991, Nodular chert from the Arbuckle Group, Slick Hills, SW Oklahoma: a combined field, petrographic and isotopic study: Sedimentology, v. 38, p. 857-870.

Geeslin, J. H., and H. S. Chafetz, 1982, Ordovician Aleman ribbon cherts; an example of silicification prior to carbonate lithification: Journal of Sedimentary Petrology, v. 52, p. 1283-1293.

Goldberg, K., S. Morad, I. S. Al-Aasm, and L. F. De Ros, 2011, Diagenesis of Paleozoic playa-lake and ephemeral-stream deposits from the Pimenta Bueno Formation, Siluro-Devonian (?) of the Parecis Basin, central Brazil: Journal of South American Earth Sciences, v. 32, p. 58-74.

Gómez-Alday, J. J., F. Garcia-Garmilla, and J. Elorza, 2002, Origin of quartz geodes from Lano and Tubilla del Agua sections (middle-upper Campanian, Basque-Cantabrian Basin, northern Spain): isotopic differences during diagenetic processes: Geological Journal, v. 37, p. 117-134.

Guidry, S. A., and H. S. Chafetz, 2002, Factors governing subaqueous siliceous sinter precipitation in hot springs: examples from Yellowstone National Park, USA: Sedimentology, v. 49, p. 1253-1267.

Guthrie, G. D., D. Bish, and R. C. Reynolds, 1995, Modeling the X-ray diffraction pattern of opal CT: American Mineralogist, v. 80, p. 869-872.

Hay, R. L., 1968, Chert and its sodium-silicate precursors in sodium-carbonate lakes of east Africa: Contributions to Mineralogy and Petrology, v. 17, p. 255-274.

Hay, R. L., and T. K. Kyser, 2001, Chemical sedimentology and paleoenvironmental history of Lake Olduvai, a Pliocene lake in northern Tanzania: Geological Society of America Bulletin, v. 113, p. 1510-1521.

Heaney, P. J., 1995, Moganite as an indicator for vanished evaporites: a testament reborn?: Journal of Sedimentary Research A: Sedimentary Petrology & Processes, v. A65, p. 633-638.

Henchiri, M., and N. Slim-S'Himi, 2006, Silicification of sulphate evaporites and their carbonate replacements in Eocene marine sediments, Tunisia: two diagenetic trends: Sedimentology, v. 53, p. 1135-1159.

Hesse, R., 1989, Silica diagenesis: origin of inorganic and replacement cherts.: Earth Science Reviews, v. 26, p. 253-284.

Jones, B., and R. W. Renaut, 2007, Microstructural changes accompanying the opal-A to opal-CT transformation: new evidence from the siliceous sinters of Geysir, Haukadalur, Iceland: Sedimentology v. 54, p. 921-949.

Jones, B., R. W. Renaut, and M. R. Rosen, 1996, High-temperature (W901C) calcite precipitation at Waikite Hot Springs, North Island, New Zealand: Journal of the Geological Society of London, v. 153, p. 481-496.

Jones, B. F., S. L. Rettig, and H. P. Eugster, 1967, Silica in alkaline brines: Science, v. 158, p. 1310-1314.

Jones, J. B., and E. R. Segnit, 1971, The nature of opal. Part 1: Nomenclature and constituent phases: Journal of the Geological Society of Australia v. 18, p. 57-68.

Keene, J. B., 1983, Chalcedonic quartz and occurrence of quartzine (length-slow chalcedony) in pelagic sediments: Sedimentology, v. 30, p. 449-454.

Knauth, L. P., 1979, A model for the origin of chert in limestone: Geology, v. 7, p. 274-277.

Knauth, L. P., 1994, Petrogenesis of chert: Reviews in Mineralogy and Geochemistry, v. 29, p. 233-258.

Knauth, L. P., and S. Epstein, 1976, Hydrogen and oxygen isotope ratios in nodular and bedded cherts: Geochimica et Cosmochimica Acta, v. 40, p. 1095-1108.

Knauth, L. P., and D. R. Lowe, 2003, High Archean climatic temperature inferred from oxygen isotope geochemistry of cherts in the 3.5 Ga Swaziland Supergroup, South Africa: Geological Society of America Bulletin, v. 115, p. 566-580.

Krainer, K., and C. Spotl, 1998, Abiogenic silica layers within a fluviolacustrine succession, Balzano volcanic complex, Northern Italy - A Permian analogue for Magadi-type cherts: Sedimentology, v. 45, p. 489-505.

Mackenzie, F. T., and R. Gees, 1971, Quartz: synthesis at earth-surface conditions: Science, v. 173, p. 533-535.

Maliva, R. G., 1987, Quartz geodes; early diagenetic silicified anhydrite nodules related to dolomitization: Journal of Sedimentary Petrology, v. 57, p. 1054-1059.

Marin, J., M. Chaussidon, and F. Robert, 2010, Microscale oxygen isotope variations in 1.9 Ga Gunflint cherts: assessments of diagenesis effects and implications for oceanic paleotempera-

ture reconstructions: Geochimica et Cosmochimica Acta, v. 74, p. 1161030.

Marin-Carbonne, J., F. Robert, and M. Chaussidon, 2014, The silicon and oxygen isotope compositions of Precambrian cherts: A record of oceanic paleo-temperatures?: Precambrian Research, v. 247, p. 223-234.

Miehe, G., and H. Graetsch, 1992, Crystal structure of moganite: a new structure type for silica: European Journal of Mineralogy, v. 4, p. 693-706.

Milliken, K. L., 1979, The silicified evaporite syndrome; two aspects of silicification history of former evaporite nodules from southern Kentucky and northern Tennessee: Journal Sedimentary Petrology, v. 49, p. 245-256.

Muchez, P., P. Vanderhaeghen, H. El Desouky, J. Schneider, A. Boyce, S. Dewaele, and J. Cailteux, 2008, Anhydrite pseudomorphs and the origin of stratiform Cu–Co ores in the Katangan Copperbelt (Democratic Republic of Congo): Mineralium Deposita, v. 43, p. 575-589.

Nagy, Z. R., I. D. Somerville, J. M. Gregg, S. P. Becker, and K. L. Shelton, 2005, Lower Carboniferous peritidal carbonates and associated evaporites adjacent to the Leinster Massif, southeast Irish Midlands: Geological Journal, v. 40, p. 173-192.

Peterson, M. N. A., and C. C. Von der Borch, 1965, Chert: modern inorganic deposition in a carbonate precipitating localitty: Science, v. 149, p. 1501-1503.

Pirajno, F., and K. Grey, 2002, Chert in the Palaeoproterozoic Bartle Member, Killara Formation, Yerrida Basin, Western Australia: a rift-related playa lake and thermal spring environment?: Precambrian Research, v. 113, p. 169-192.

Rodgers, K. A., and G. Cressey, 2001, The occurrence, detection and significance of moganite (SiO_2) among some silica sinters: Mineralogical Magazine, v. 65, p. 157-167.

Scholle, P. A., and D. S. Ulmer-Scholle, 2003, A Color Guide to the Petrography of Carbonate Rocks: Grains, textures, porosity, diagenesis, v. 77: Tulsa, Okla, American Association of Petroleum Geologists Memoir, 459 p.

Siever, R., 1962, Silica solubility, 0°–200 °C., and the diagenesis of siliceous sediments: Journal of Geology, v. 70, p. 127-150.

Tucker, M. E., 1976a, Quartz replaced anhydrite nodules ('Bristol Diamonds') from the Triassic of the Bristol District: Geological Magazine, v. 113, p. 569-574.

Tucker, M. E., 1976b, Replaced evaporites from the late Precambrian of Finnmark, Arctic Norway: Sedimentary Geology, v. 16, p. 193-204.

Ulmer-Scholle, D. S., and P. A. Scholle, 1994, Replacement of evaporites within the Permian Park City Formation, Bighorn Basin, Wyoming, USA: Sedimentology, v. 41, p. 1203-1222.

Ulmer-Scholle, D. S., P. A. Scholle, and P. V. Brady, 1993, Silicification of evaporites in Permian (Guadalupian) back-reef carbonates of the Delaware Basin, west Texas and New Mexico: Journal of Sedimentary Petrology, v. 63, p. 955-965.

van den Boorn, S. H. J. M., M. J. van Bergen, W. Nijman, and P. Z. Vroon, 2007, Dual role of seawater and hydrothermal fluids in Early Archean chert formation: Evidence from silicon isotopes: Geology, v. 35, p. 939-942.

Warren, J. K., 2016, Evaporites: A compendium (ISBN 978-3-319-13511-3) Published Feb. 22, 2016: Berlin, Springer, 1854 p.

West, I., 1973, Vanished evaporites; significance of strontium minerals: Journal of Sedimentary Petrology, v. 43, p. 278-279.

West, I. M., 1964, Evaporite diagenesis in the lower Purbeck beds of Dorset [with discussion]: Proc. Yorkshire Geol. Soc., v. 34, p. 315-330.

Wheeler, W. H., and D. A. Textoris, 1978, Triassic limestone and chert of playa origin in North Carolina: Journal of Sedimentary Petrology, v. 48, p. 765-776.

Williams, L. A., and D. A. Crerar, 1985, Silica diagenesis, II. General mechanisms: Journal of Sedimentary Petrology, v. 55, p. 312-321.

Williams, L. A., G. Parks, and D. A. Crerar, 1985, Silica diagenesis, I. Solubility controls: Journal of Sedimentary Petrology v. 55, p. 301-311.

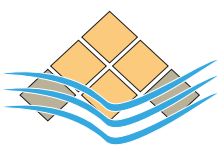

John Warren, Chief Technical Director
SaltWork Consultants Pte Ltd (ACN 068 889 127)
Kingston Park, Adelaide, South Australia 5049

www.saltworkconsultants.com